Supplementary information

Supplementary Figures

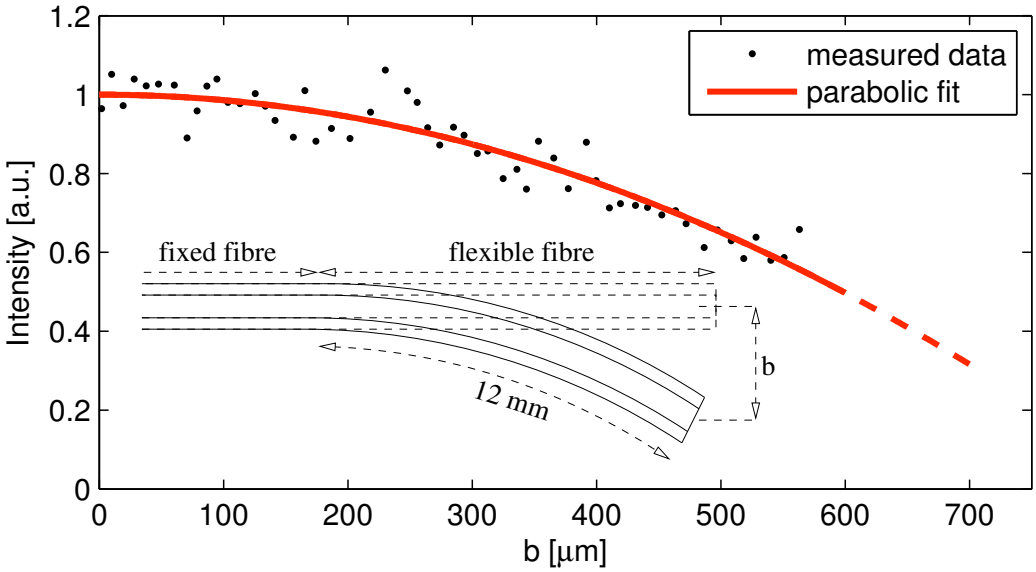

Supplementary Figure S1: **Intensity of an output mode as a function of fibre curvature.** For this demonstration we fixed the fibre near the end leaving the last segment of 12 mm flexible. After a calibration we generated a single output mode 30μm behind the fibre facet. We mechanically bent the fibre by a differential actuator and followed the intensity change of the output mode. We can conclude that the intensity drops adiabatically with the amount of curvature introduced, however the instrument would operate very well even with deviations exceeding 10s-100s of micrometers.

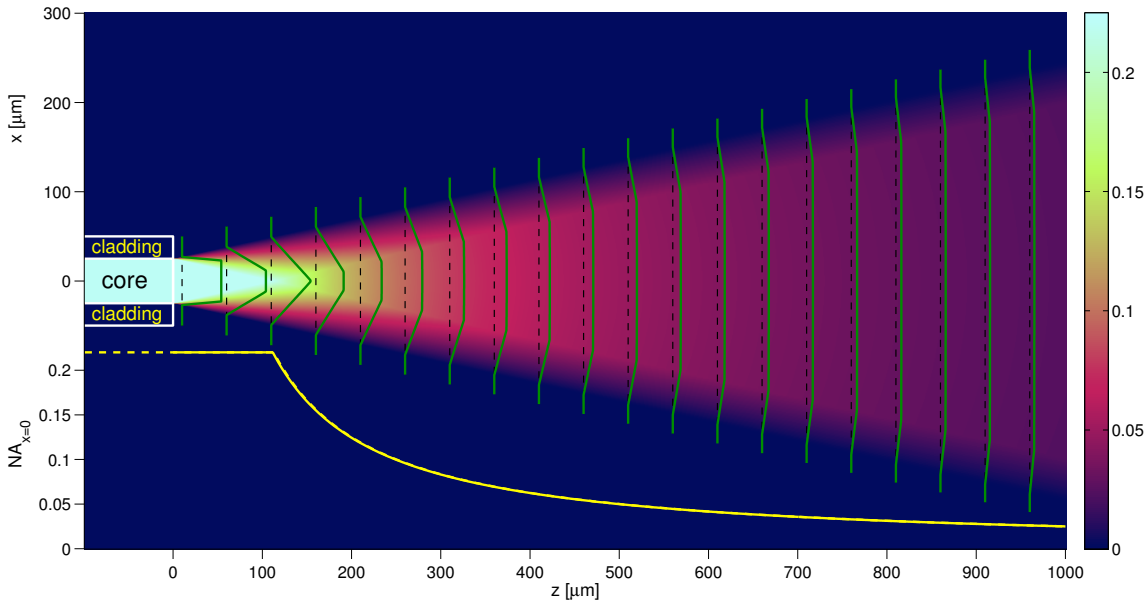

Supplementary Figure S2: **Numerical aperture of sample modes at different distance from the fibre facet**. The bottom plot demonstrates the NA evolution along the optical axis and the series of green subplots show NA profiles across different axial planes behind the fibre. The calculation is provided for fibre parameters used in our experiments (NA=0.22, core diameter of d=50 μm). As shown, the maximal NA (corresponding to the highest spatial resolution) can be achieved only in a cone with a base corresponding to the fibre core and the height of $d/2\text{NA} \approx 110$ μm. Further increasing the depth leads to growth of the field of view, but limited NA. Configuring the system to image the far-field (large distances from the fibre) would bring uniform spatial resolution across the sample plane.

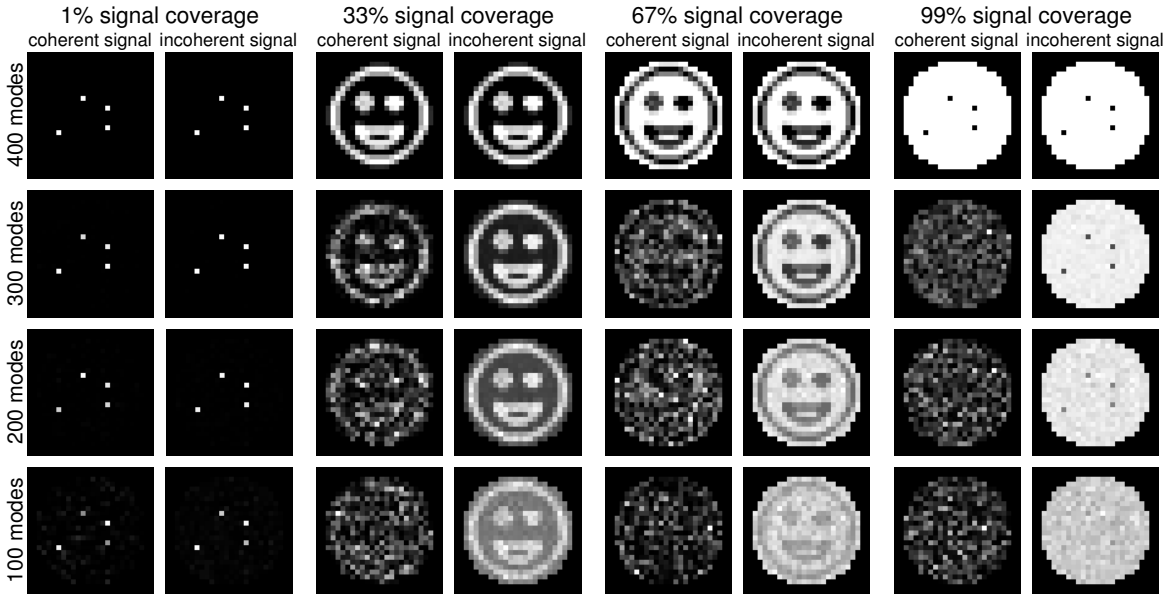

Supplementary Figure S3: **Performance of imaging with incomplete transformation basis.** This simulation outlines the influence of incomplete non-unitary transformations to the imaging performance. Individual rows show resulting images obtained while using all or only a fraction of transformation base vectors during the image reconstruction. These results show the crucial role of orthogonality between propagating modes. Within our system the orthogonality can be achieved only if light is coupled into the fibre in both polarizations and both phase and amplitude modulation is provided. We consider a system that allows 400 modes to propagate. We generate a random orthogonalised transformation matrix to simulate a random optical system. Optical fields behind the optical system (at the SLM plane), corresponding to the sample field, are generated using the transformation matrix. For the image reconstruction an inverse transform is used, however this contains only a portion of the base vectors (SLM modes), with the remaining ones set to zero. A simulation is provided for spatially coherent and incoherent sample fields separately. In the case of fluorescent imaging, the detected signal is natively incoherent, and crosstalk is caused by excitation of sample parts outside the area of the sample mode. In the case of bright-field/dark-field imaging, it is highly advantageous to provide spatially-incoherent illumination either by rapid beam-steering or transmission through a rotating diffuser as this leads to crosstalk with the form of a uniform background rather than speckled noise. As seen, the contrast reduction is strongly correlated with the amount of bright sample modes (signal coverage), that is specific for different imaging methods. Fluorescence imaging typically operates at very low signal coverage and even with a strongly reduced transformation basis would give acceptable results. The quality of fluorescent imaging typically suffers elsewhere due to photobleaching, very weak signals (photon noise), electronic disturbance etc. On the other hand, bright-field imaging requires very high signal coverage, and thus suffers significantly with incomplete transformation basis. The contrast is proportional to the number of modes used, with accurate imaging only appearing for the complete basis.

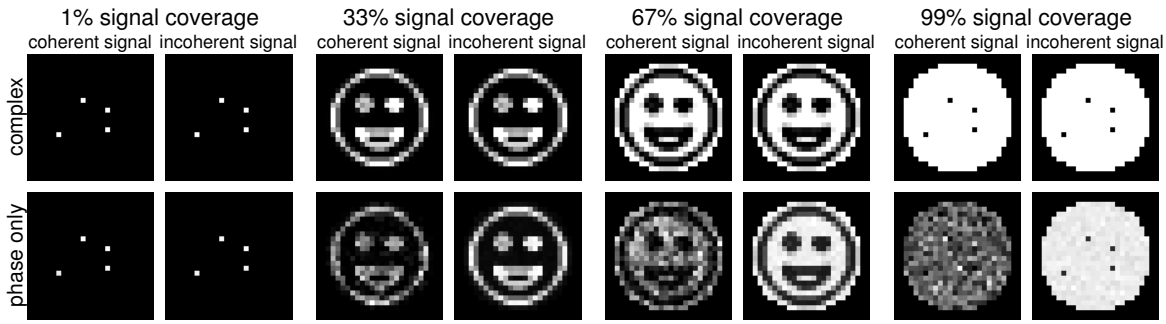

Supplementary Figure S4: **Performance of imaging using phase-only modulation.** Using phase-only SLM modulation instead of full complex modulation also significantly influences the quality of imaging. We have simulated this influence by setting absolute value of each element of the inverse transform equal to 1. The imaging quality is affected particularly for higher signal coverage (bright-field). Providing amplitude modulation is typically accompanied with very high power losses[20]. Therefore in cases with a very low signal coverage (fluorescence imaging) the amplitude modulation is not practical.

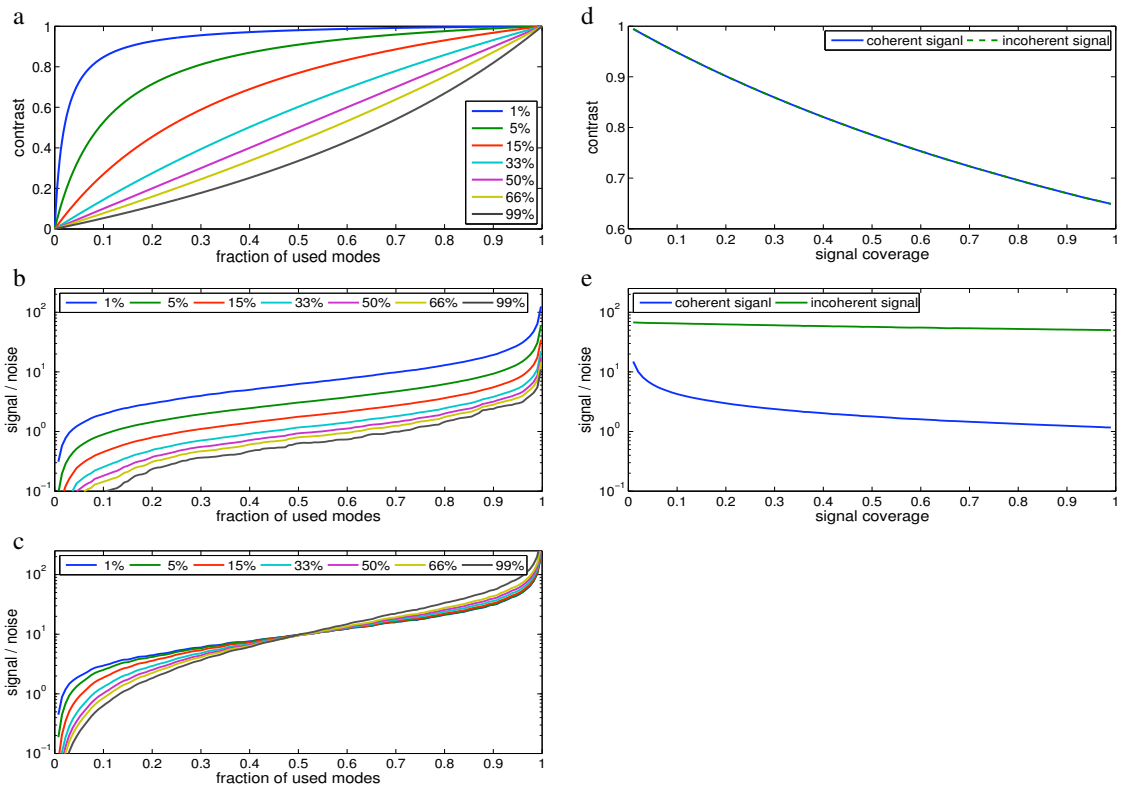

Supplementary Figure S5: **Quantitative characteristics of the imaging performance with incomplete transformation basis or phase-only modulation.** Results represent averaged values obtained from 10 000 simulations for each case. **a**, Imaging contrast as a function of number of modes used. Individual plots correspond to different signal coverages. Results for the coherent and the incoherent cases are identical. **b** and **c**, Signal / noise ratio of the imaging for the case of coherent and the incoherent light respectively as a function of number of used modes. **d**, Contrast of the images obtained using phase-only modulation as a function of signal coverage. **e**, Signal/noise ratio of the images obtained using phase-only modulation as a function of signal coverage.

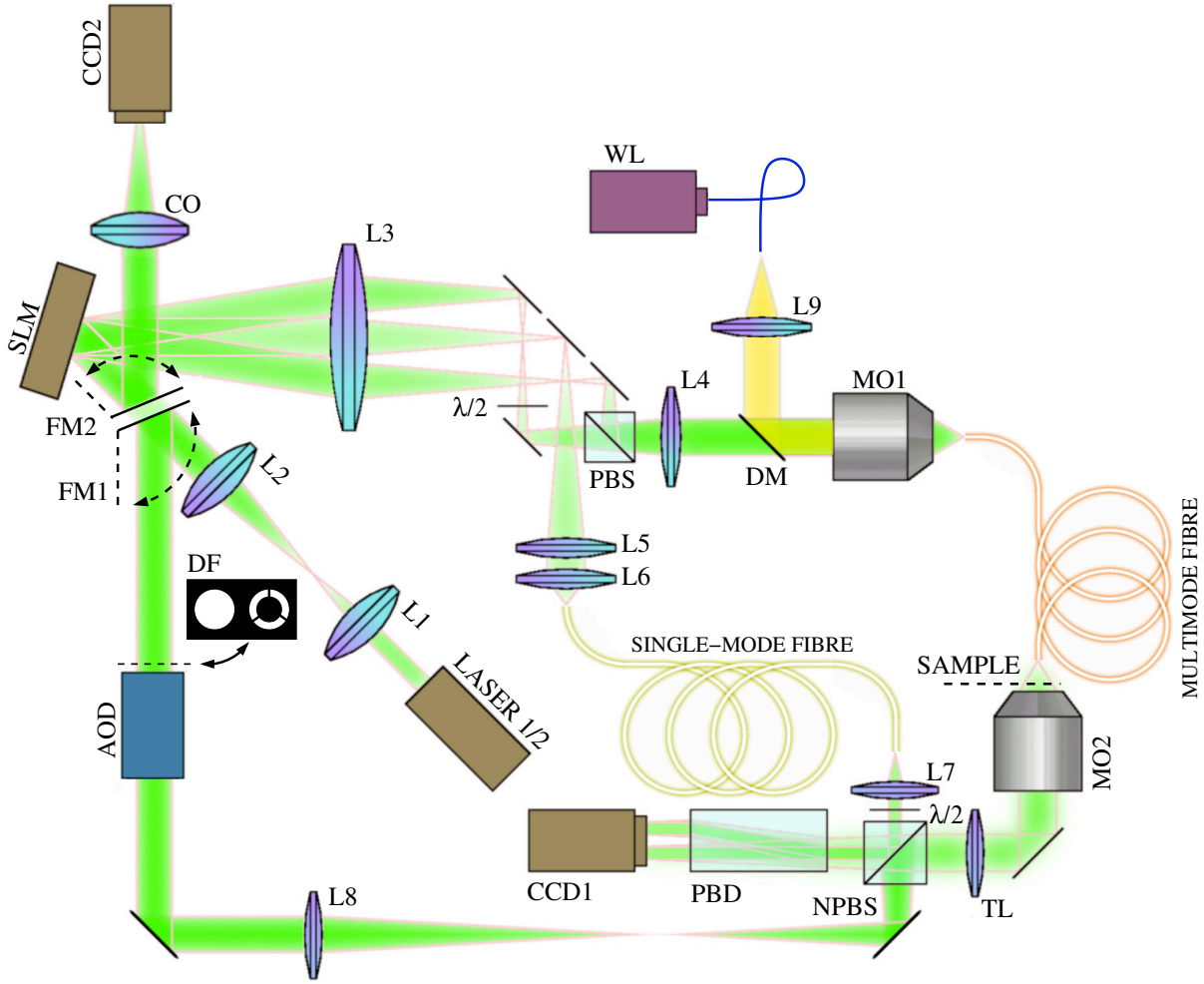

Supplementary Figure S6: **Rigorous diagram for the experimental geometry designed for bright-field and dark-field imaging.** LASER 1/2 - IPG YLR-10-1064-LP-SF λ = 1064 nm; L1 - Thorlabs AC254-150-C-ML, f=150mm; L2 - Thorlabs AC254-300-C-ML, f=300mm; SLM - Boulder Nonlinear Systems, model P512 1064, with high speed chip option; L3 - Thorlabs AC254-400-C-ML, f=400mm; $\lambda/2$ - Thorlabs WPMH05M-1064; PBS - Thorlabs, PBS253; MO1 - Mitutoyo M Plan Apo 20x 0.42 NA; L4 - Thorlabs AC254-200-C-ML, f=200mm; multimode fibre - Thorlabs M14L01, 1m long, with core diameter of 50μm, allowing $\approx$ 400 propagating modes at the wavelength of 1064 nm; CCD1 - Basler pi640-210gm; MO2 - Newport M 20x, 0.40 NA; TL - Thorlabs AC254-200-C-ML, f=200 mm. The central optical pathway propagating behind the SLM is used as an external reference[20] for the calibration eliminating problems related to the use of an internal reference[2] - zero-intensity regions in the speckled signal and ambiguity of its phase distribution. Single-mode fibre - Thorlabs p3-830A-FC-2; L5 - Thorlabs AC254-200-C-ML, f=200mm; L6 - Thorlabs C260TME-C, f=15mm; L7 - Thorlabs A240TM-C, f=8mm; NPBS - Thorlabs BS015; PBD - Thorlabs BD40; AOD - IntraAction, DTD-274HD6M; FM1 and FM2 - flipping mirrors; L8 - Thorlabs AC254-200-C-ML, f=200mm; CO - Computar M6Z1212-3S; CCD2 - Basler pi640-210gm; DF - home made dark-field filter; WL - Thorlabs OSL1; L9 - Thorlabs AC254-150-A-ML, f=150mm; DM - custom-manufactured dichroic mirror from the Institute of Scientific Instruments, Brno.

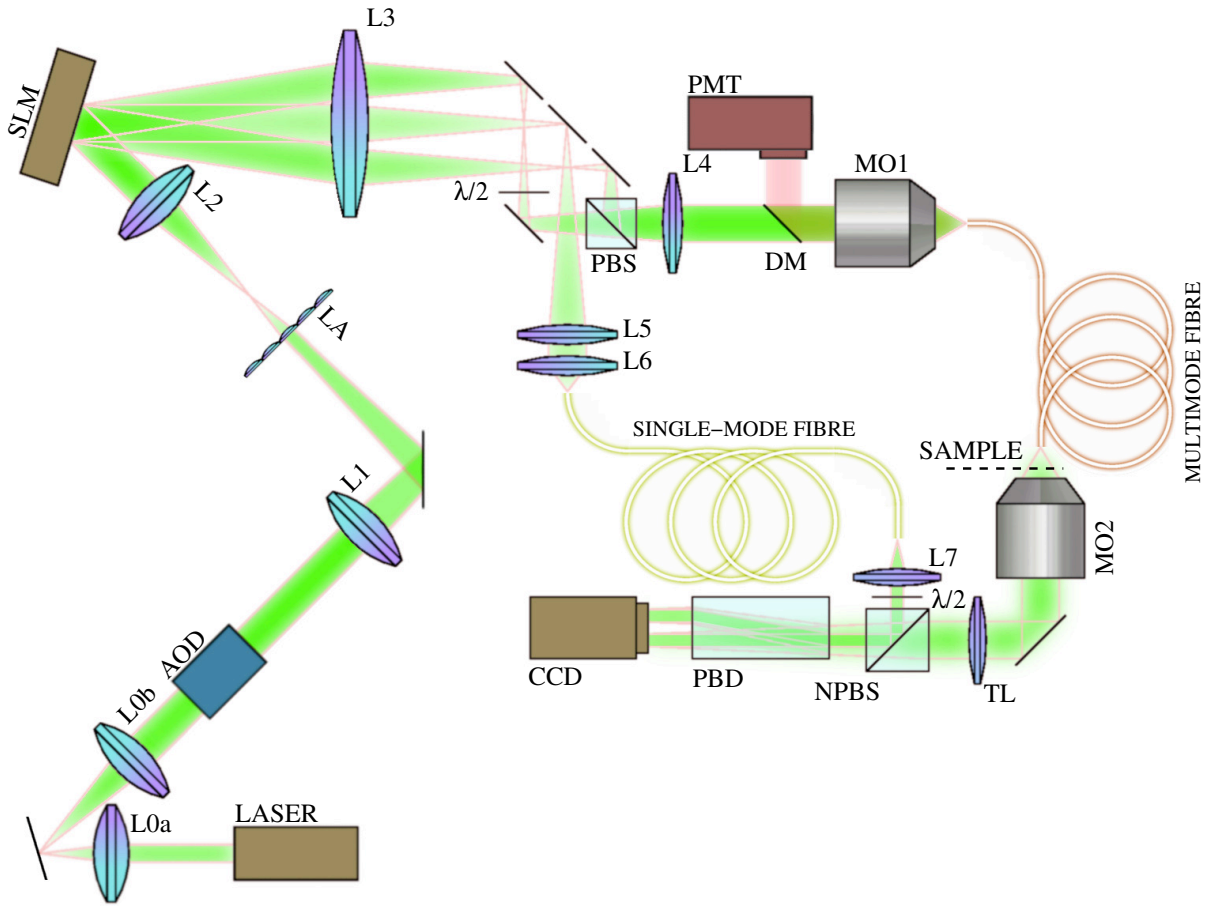

Supplementary Figure S7: **Rigorous diagram for the experimental geometry designed for fluorescence imaging showing all optical elements used.** LASER - Coherent Verdi V5, $\lambda = 532$ nm; L0a - Thorlabs AC254-050-A-ML, f=50mm; L0b - Thorlabs AC254-200-A-ML, f=200mm; AOD - IntraAction, DTD-274HD6M; L1 - Thorlabs AC254-500-A-ML, f=500mm; LA -Thorlabs MLA150-5C; L2 - Thorlabs AC254-400-A-ML, f=400mm; SLM - Boulder Nonliner Systems, model P512 0532, with high speed chip option; L3 - Thorlabs AC254-500-A-ML, f=500mm; PBS - Thorlabs PBS251; L4 - Thorlabs AC254-300-A-ML, f=300mm; MO1 - Leiz Wetzlar 10/0.25; multimode fibre - Thorlabs M14L02, 2m long, core diameter of 50μm; MO2 - Newport M 20x, 0.40 NA; TL - Thorlabs AC254-200-A-ML, f=200 mm; L5 - Thorlabs AC254-300-A-ML, f=300 mm; L6 - Thorlabs C260TME-A, f=15mm; single-mode fibre - Thorlabs P1-460A-FC-2; L7 - Thorlabs A240TM-A, f=8mm; NPBS - Thorlabs BS013; PBD - Thorlabs BD40; CCD - Basler pi640-210gm; DM - dichroic mirror custom-manufactured at Institute of Scientific Instruments, Brno; PMT - Hamamatsu H6780-20.

Supplementary discussion

Orthogonality in bright-field imaging and synthesis of imaging hologram

Let us assume we can provide an ideal phase and amplitude modulation at the SLM and that the SLM is uniformly illuminated from LASER 1 with a flat wavefront: $f_0(x,y) = 1$. After calibration we can set the SLM to generate a field along the SLM $f_i(x,y)$ such that after propagation through the fiber a perfect focus F_i is formed in the sample plane at a selected position i. A series of such optimally focussed beams - sample modes - can serve as an orthogonal basis in which we describe any optical field within a sample. Fields f_i and F_i are related by the orthogonal fibre transformation $\mathcal{T}$, which was measured by the calibration procedure: $f_i = \mathcal{T}\{F_i\}$ [20]. Let us also assume that the modulation efficiency for generating individual sample modes is equal for all of them, regardless of their position:

$$\iint\limits_{SLM} f_i^*(x,y) \cdot f_i(x,y)\ \mathrm{d}x\mathrm{d}y = 1 \text{ for } i \in <1,n>, \tag{S1}$$

where n is the number of modes allowed to propagate within the fibre. If a second laser beam with a field magnitude a_i propagates from the opposite direction (LASER 2) to form a perfect focus at the same position within the sample ($F^i = F_i^*$; * represents the complex conjugation), the light will propagate through the fibre onto the SLM as a phase-conjugate field where we get $f^i(x,y) = f_i^*(x,y)$. Passing the SLM, the field is modulated as $f_i^i(x,y) = f_i^*(x,y) \cdot f_i(x,y)$. Fourier transforming this field with a lens (CO), at the optical axis we get field value of

$$S_i^i = \mathcal{F}\{a_i \cdot f_i^i(x,y)\}|_{u,v=0} = a_i \cdot \iint\limits_{SLM} f_i^*(x,y) \cdot f_i(x,y)\ \mathrm{d}x\mathrm{d}y = a_i, \tag{S2}$$

where $\mathcal{F}\{\alpha\}$ is a Fourier transform of α between spatial coordinates x, y along the SLM plane and spatial frequencies u, v along the focal plane of CO. Mathematically, formula (S2) represents a scalar product of the field $f_i^*(x,y)$ with itself. If the beam with field magnitude a_j from LASER 2 is focused on another location along the sample plane ($F^j = F_j^*$), such that the beam extent does not overlap with F^i, the fields F^i and F^j are orthogonal and since the orthogonality within the optical system is conserved [2] the resulting fields f^i and f^j are orthogonal as well, therefore for the on-axis signal at the focal plane of CO we get:

$$S_i^j = a_j \cdot \iint\limits_{SLM} f_j^*(x,y) \cdot f_i(x,y)\ \mathrm{d}x\mathrm{d}y \equiv 0. \tag{S3}$$

In general, $S_l^k = a_l \cdot \delta_l^k$, where δ_l^k is the Kronecker's delta. As any optical field $\bar{F}$ in the image plane within the range of accessible spatial frequencies and field of view can be expressed as a superposition of sample modes $\bar{F} = \sum\limits_{q=1}^{N} a_q \cdot F^q$, while applying the modulation of f_k at the SLM chip, the signal S_k is proportional to the contribution a_k of fundamental mode F^k to the field $\bar{F}$. Hence we can directly observe intensity of one point within the sample chamber regardless of the light distribution across the remaining area. This is only possible if the measured fibre transformation $\mathcal{T}$ is orthogonal, i.e. it was measured with a complete set of base vectors (SLM modes), covering both polarizations and the entire light signal (at the given wavelength) that can be within the geometry coupled into the fiber. The calibration however can only be acquired with a limited number of SLM modes that is given by the SLM parameters. If a higher number of modes are allowed to propagate in the system, the transformation matrix is incomplete and thus not orthogonal/unitary. In Supplementary Figure S3, we show the consequences if orthogonality is not maintained. In orthogonal systems, light propagating within remaining modes is distributed around the focal plane of CO but, as explained above, does not contribute to the on-axis intensity at the central point. It can be shown that the whole signal is confined within a finite area - active zone - with a diameter not exceeding 2× the diameter of the fiber central core magnified by the MO1 - CO telescope. An additional linear modulation (blazed grating, tilt) can be added to the modulation of f_k to shift the whole active zone off-axis.

To simultaneously observe a number of sample modes, the area of detector CCD2 is split into a series of non-overlapping regions such that each could accommodate one active zone. An automized procedure is employed to provide a set of blazed gratings such that the central point of one testing active zone is

sequentially aligned with very high precision onto a central pixel within each region of CCD2 - an active pixel. Spacing between individual active pixels must be large enough so that neighboring active zones do not interfere with their signals. A static imaging hologram is synthesized as a superposition of individual modulations $f_1 ... f_n$, each carrying a different blazed grating to center the corresponding active zone at a different region of CCD2. The imaging hologram carries both phase and amplitude modulation. The SLM used in our geometry is however a phase-only modulator. As shown in Supplementary Figure S4, using phase-only modulation (amplitude distribution is ignored) results in a reduction of contrast, most significantly influencing bright-field imaging. Complex modulation with a phase-only SLM, is typically very lossy and in our geometry is used for for bright-field imaging only. To generate holograms featuring amplitude modulation we follow reference[27]. Employing the imaging hologram the system is set for imaging, and the sample image is reconstructed from intensity values measured by individual active pixels.

Reduction of instrument diameter

In this paragraph we estimate the amount of information that can be transferred via various available approaches and compare the results to the case of step-index multimode optical fibre. The number of optical modes corresponding to the following examples is very high compared to the experiments presented in this paper and one would need spatial light modulators of a very high speed and pixel resolution to allow video-rate imaging at these scales. These examples however clearly point the potential reduction of collateral damage when our technique is deployed.

The footprint of a typical flexible endoscope is dictated by the dimensions of the anterior optics, however even the image guiding fibre can represent a considerable limitation. In a typical fibre bundle, 30,000 guiding cores of $NA = 0.35$ are contained within a circular area of 720 μm in diameter[13,14]. Due to the *in situ* sampling however, the available information content of the transferred image is reduced by factor of 4 as one can only access the 2-D spatial spectrum domain up to one half of the sampling frequency (the Nyquist frequency) along each dimension. The diameter of a multimode fibre core d capable of transferring an equal amount of optical modes N can be estimated as[35]:

$$d = \frac{\lambda\sqrt{N}}{2NA}. \tag{S4}$$

At the wavelength of $\lambda = 0.5$ μm and for the same NA, the resulting diameter is $\approx 61\mu$m.

Similarly a rigid endoscope described in[16] with $NA = 0.9$ and instrument diameter of 5mm can provide an image of a circular area of 400μm in diameter with lateral spatial resolution of $1 - 2\mu$m at the wavelengths of $\lambda = 670$nm. Based on (S4) multimode fibre with equivalent NA and with diameter of $66 - 132\mu$m could bring equivalent imaging quality.

Another alternative technology employs scanning a single-mode fibre across the imaging plane. A multimode fibre with analogous NA and core size corresponding to the scanned area would bring an analogous performance without any additional anterior optics and substantial mechanical actuators responsible for physical instrument dimension of the order of one millimeter[17,18].

Spectral purity requirements for laser sources

In this section we estimate the limit for the bandwidth of a laser source that could be used for this technique. The minimal optical distance through the fibre (photon traveling directly along the fibre axis) is:

$$s_{min} = nl, \tag{S5}$$

where n is the refractive index of the fibre and l is the fibre lengths. The maximal optical distance (photon 'bouncing' at core/cladding interface at the critical angle) is:

$$s_{max} = \frac{nl}{\cos(\frac{NA}{n})}, \tag{S6}$$

where NA is the numerical aperture. The coherence lengths of the laser for 50% of reduction in fringe visibility is given as:

$$L = \frac{c}{\Delta f}, \tag{S7}$$

where Δf is the frequency bandwidth. To control the light output we need this value significantly exceeding the difference between the maximal and minimal distance (S5) and (S6) respectively, leading to:

$$\Delta f \ll \frac{c}{nl\left[\frac{1}{\cos(\frac{NA}{n})} - 1\right]}. \tag{S8}$$

In our system $\Delta f \ll 9$ GHz. In turn these equations can assist to estimate the maximal lengths of fibre that we can use with given laser bandwidth. For example a femtosecond laser source allowing two-photon excitation with bandwidth of $\approx$ 2THz could only be used with fibres no longer that 1cm.